International Journal of Rock Mechanics & Mining Sciences 77 (2015) 246–256

Contents lists available at ScienceDirect

International Journal of Rock Mechanics & Mining Sciences

journal homepage: www.elsevier.com/locate/ijrmms

Models for the effect of rising water in abandoned mines on seismic activity

Neville Fowkes [a,*], G. Hocking [b], D.P. Mason [c], C.P. Please [d], R. Kgatle [c], H. Yilmaz [e], N. van der Merwe [e]

[a] School of Mathematics and Statistics, University of Western Australia, Crawley, WA 6009, Australia
[b] Mathematics and Statistics, FSE Murdoch University, Murdoch, WA 6150, Australia
[c] School of Computational and Applied Mathematics, University of the Witwatersrand, Johannesburg, Private Bag 3, WITS 2050, South Africa
[d] Oxford Centre for Collaborative Applied Mathematics, University of Oxford, United Kingdom
[e] School of Mining Engineering, University of Witwatersrand, Johannesburg, South Africa

ARTICLE INFO

Article history:
Received 10 June 2013
Received in revised form
16 April 2015
Accepted 19 April 2015
Available online 16 May 2015

Keywords:
Fault slip
Seismicity
Water movement in joints
Abandoned mines

ABSTRACT

The old closed gold mines on the Witwatersrand are flooding and there is concern that the water may seep into stable faults in the district and destabilise them, thus leading to greater seismic activity. The simple deterministic models described here suggest that the time span for water movement into such faults within a distance of 3000 m is likely to be of the order of months and that the hydrostatic pressure buildup within the filled cracks is likely to significantly increase the risk of fault slip. These results appear to be consistent with available observations as documented by Goldbach [20]. The simple models predict a linear decrease in the effective coefficient of friction of the water filled fault with water depth with a reduction of up to 30% possible. Furthermore, and importantly, slip is predicted to occur along joints and faults not previously prone to slip because of their unfavored orientation.

1. Introduction

In gold mining areas water collects in the shafts and is pumped out to facilitate the operations, but once the mining activity has ceased the pumping is also discontinued and so water accumulates. The depth of water in such abandoned shafts and tunnels can typically increase at up to 1–2 m per day under wet conditions. The concern is that this water may then seep into faults that are hydrologically connected to the mining network thus lubricating them, and this could lead to an increased incidence of seismic events subsequently.

The first issue is whether or not water will reach fault sites over time spans of public concern (say 10 years). This will be addressed in Section 2. Then in Section 3 we investigate the effect of water entry on fault slip. Explicitly we determine the change in the effective coefficient of friction brought about by water entry. Finally there is a Results and Discussions section. Much of the detailed mathematical analysis is relegated to the Appendices.

The simple mechanistic models developed here are generic in type and as such serve to address the general issues; assessments for particular mining sites would require the results obtained here be plugged into complete hydraulic and stress models of the site.

We will first briefly review work in the area of mining-induced seismicity and then go on to describe observations on the effects of water entry on seismicity.

1.1. Mining-induced seismicity

Mining-induced seismicity and its hazardous manifestation, rockbursts, were first encountered in the early 1900s when extensive mining stopes reached depths of several hundred meters in the Witwatersrand Basin in South Africa [1,2]. Since that time mining depths have significantly increased, with the deepest gold mines now exceeding 3.5 km, resulting in an increased incidence of rockbursts. Also cities and towns have developed in the mining districts so that the number of casualties has continued to increase, see Fig. 1. Several mining related seismic events with $M > 5$ have been recorded in South Africa causing serious damage to surface structures, with the largest occurring in the Klerksdorp district on 9 March 2005. The $M = 5.3$ main shock and aftershocks shook the town of Stilfontein, causing serious damage to several buildings and minor injuries to 58 people, see Durrheim [2].

* Corresponding author. Tel.: +89 64883355.
E-mail addresses: fowkes@maths.uwa.edu.au (N. Fowkes), g.hocking@murdoch.edu.au (G. Hocking), David.Mason@wits.ac.za (D.P. Mason), please@maths.ox.ac.uk (C.P. Please), mrr.kgatle@gmail.com (R. Kgatle).

http://dx.doi.org/10.1016/j.ijrmms.2015.04.011
1365-1609/

Durrheim expressed concern that the flooding of abandoned mines may increase the risk.

The role of geological discontinuities in seismicity has long been recognised and the landmark paper by Cook et al. [4] is one of the earliest outcomes of the research in this area. Commencing in 1982 there have been a specialised series of symposia on "Rockbursts and Seismicity in Mines"; to date there have been eight such symposia. A number of papers in the first symposium highlighted the influence of geological discontinuities in seismicity [5–12]). The symposium participants in general agreed that the majority of large (magnitude, $M > 2$), damaging seismic events are associated with major fault planes and dyke contacts that are influenced by nearby mining activity, whereas smaller seismic events are normally correlated with mining only. Fig. 2 shows the increased number of rockbursts when the mining is in the proximity of faults and dykes.

Based on seismic observations in five deep gold mines in the Far West Rand using in-mine arrays of geo-phones Richardson and Jordan [13] were able to characterise the above two types of mining-induced seismicity events which they designated as Type A and Type B.

Type A events are caused by intact rock fracture and generally occur within 100 m of the active mining face or development tunnel and are caused by dynamic stress associated with blasting, or quasi-static stress perturbations caused by excavation. Such events are characterised by a small moment-magnitude ($M < 0$) (as defined by [14]), high frequency ($f > 100$ Hz) spectral response occurring soon after (< 30 s) the initiating event. The source-scaling (frequency vs magnitude) relations are similar to those seen in hydrofracturing events. Type A events are not of direct interest here.

Type B events represent friction dominated slip in existing shear zones such as joints, faults and dykes and are distributed throughout the active mining region. These events have a cut off lower magnitude of $M \approx 0$ but can be of large magnitude ($M > 2$) and produce a low frequency spectral response with a cut off frequency of approximately 200 Hz which is attributed to the critical-patch size for nucleation of shear failure, see Dieterich [15] and Aki [16]. The source-scaling properties of these events are similar to those of normal tectonic earthquakes; the Gutenberg–Richter power-law frequency vs moment relation observed for tectonic earthquakes also holds for Type B events, see Richardson and Jordan [13]. Type B events typically have a higher S/P amplitude ratio than those of Type A.

There have been a number of additional and more detailed experimental seismic investigations by the JAGUARS group (Japanese-German Underground Acoustic Emission Research Group) in the deep (3.5 km) Mponeng gold mine in the Far West Rand district, see Kwiatek et al. [17,18] and Plenkers et al. [19]. The group used a 'JAGUARS network' consisting of a triaxial accelerometer and eight AE acoustic sensors installed in the mine. The results obtained confirm the classification; the Type B events of specific interest here can be reliably identified using their seismic signature.

1.2. Fluid-induced seismicity

In order to create an awareness that fluid-induced seismicity would become increasingly important in South Africa when closed mines are allowed to flood Goldbach documented a number of cases of fluid-induced seismicity some of which will be described briefly here; for more details see Goldbach [20].

1.2.1. The Goldbach abandoned mine example

Goldbach described a case where a worked-out part of a deep-level South African gold mine was allowed to flood next to an active mining area, see Fig. 3. Seismicity was recorded over a 5-year period

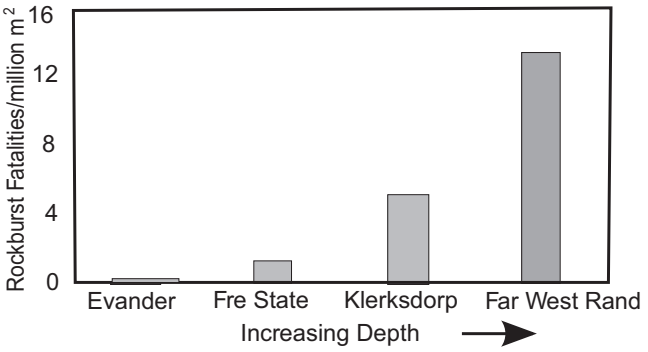

Fig. 1. Fatality rates in South African gold mining districts in the order of increasing depth between 1990 and 1997 (modified after [3]).

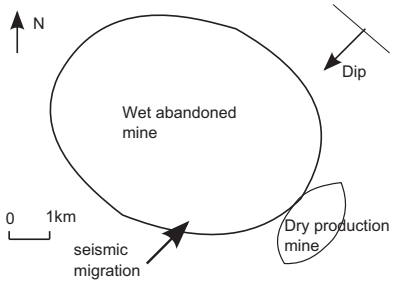

Fig. 3. The Goldbach abandoned mine example: schematic of the mine plan showing the large abandoned mine which was flooding and the smaller adjacent dry production mine. There is a dip in the geological structure so that the old mine filled up to the surface from SW to NE. Seismic events migrated up-dip as the mine filled [20].

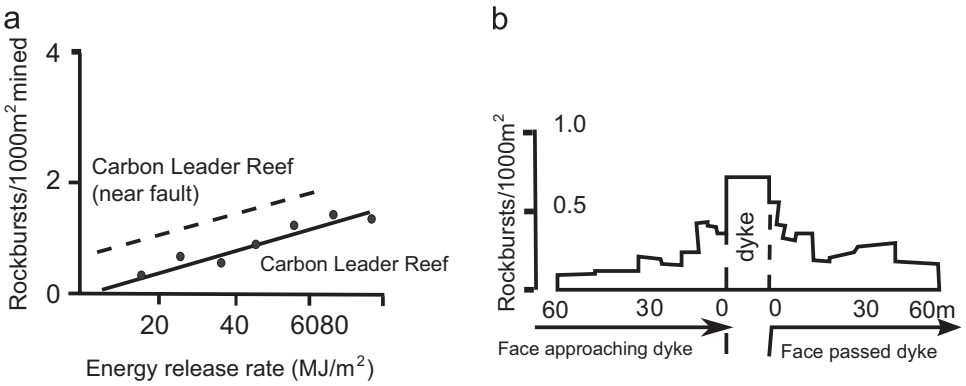

Fig. 2. Effect of proximity to faults/dykes on rockburst incidence [3].

commencing in July 1999 in both the "dry" production area and the "wet" flooding area. Additional seismic activity was noticed in the flooded section. Seismicity increased exponentially and migrated up-dip over a period of approximately 18 months in the wet area. On the other hand, seismic events occurring in the dry mining area displayed an almost constant event rate over this period.

Fig. 4 shows the elevation of the water level together with the depth of the seismic event locations in the flooding area as a function of time. A dense cluster of seismic events is observed approximately 14 months after flooding commenced. Then the locations of these seismic events migrated upwards initially rapidly, but later at a slower rate, eventually coinciding with the elevation of the water level. Fig. 4 indicates that complete flooding took place in approximately 62 months which means that water levels on average rose by approximately 75 cm/day.

Evidently the distance of separation between the dry production area and the wet abandoned area >100 m is such that most of the mining events in the wet area would have been Type B frictional slip events, whereas in the dry area most of the events were likely to have been mining generated Type A events. Goldbach noted that despite the flooding area having been mined out long ago, it generated larger seismic events than the neighbouring mining area, again consistent with Type B events as noted earlier. Furthermore he found that seismic events in the wet area occurred randomly throughout the day and week as one would expect from Type B events, whereas events in the dry area followed a typical mining process pattern.

1.2.2. Other examples of fluid-induced seismicity

To the authors' knowledge there have been no other useful quantitative seismic observations of abandoned mines however Goldbach [20] reported that fluid-induced seismicity has been observed in the filling of reservoirs, oil-well stimulation and hydrothermal fields; some of these examples will be briefly described here.

Rocky Mountain Arsenal: A 3671 m deep disposal well was completed by the U.S. Army at the Rocky Mountain Arsenal in 1961, and four phases of waste fluid injection were undertaken between 1962 and 1966, see Fig. 5 [21]. A significant correlation was noted between the volumes of fluid pumped into the Rocky Mountain Arsenal wellbore and the number of earthquakes detected. Note that there was roughly a time delay of 1 month between injection rate and the seismic response. The seismicity was observed to continue for almost two years after fluid injection was stopped in early 1966, with the three largest seismic events ($M=5.0$–5.5) taking place a year later over a period of eight months. Seismic activity also ceased shortly after the earthquakes of 1967. The area reportedly had "no evidence of seismic activity before 1962".

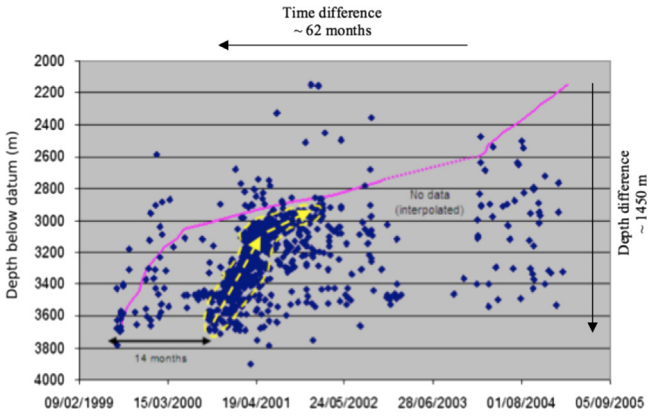

Fig. 4. Elevation of water level (solid line) and depth of seismic event locations (diamond symbols) in the flooding area. Note the initial delay of 14 months and the upward migration of a cluster of seismic events (dashed line) between September 2000 and February 2002 [20].

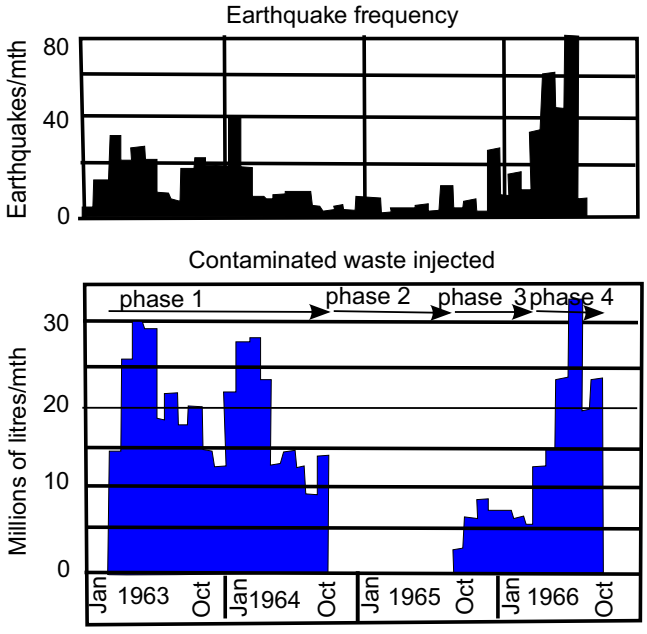

Fig. 5. Comparison between Denver earthquake activity and the fluid injection phases at the Rocky Mountain Arsenal [21]. Note the significant correlation between injection rate and seismic activity. Also note that there is about a 1 month delay between injection and seismic response.

Rangely Colorado oil field: Gibbs et al. [23] noted that water injection into oil wells to stimulate secondary oil production increased the seismic activity in the Rangely Colorado oil field. The wells were drilled into the oil bearing sandstone 350 m thick, 1900 m below the surface. A large number of seismic events coincided with a fault that cut through the centre of the oil field. The frequency of seismicity was found to increase with the fluid injection rate and the response time was of the order of months or less. Further experimental and computational work by Raleigh et al. [24,22] on Rangely demonstrated the feasibility of the use of water injection for earthquake control.

Matsushiro experiment: Ohtake [25] reported a significant amount of induced seismicity during a fluid injection scientific experiment undertaken at Matsushiro, Japan in 1970. Water was pumped into an 1800 m deep wellbore over a period of 1 month. The borehole intersected the Matsushiro fault zone. The time delay between the initiation of fluid injection and the first recorded seismic activity was nine days. The events appeared to localise along the projected fault surface.

Katse Dam: Brandt [26] observed that as the water level in the reservoir of the Katse Dam rose, the seismicity closely followed the changes in the reservoir level with a delay of about one month between changes in the reservoir level and the eventual occurrence of the reservoir-induced seismicity.

The above evidence as documented by Goldbach is compelling and suggests that flooding in deep mines can produce increased seismic activity in nearby faults with the response time typically ranging over days to months after flooding. We will set up simple models to further examine the issues.

2. Water flow in cracks and crack networks

2.1. Previous work on flow in cracks

It is useful to distinguish between faults and dykes which are normally thick cracks >5 mm containing material either crushed due to sliding, or transported to the crack, and joints which are

thin cracks (< 5 mm) for which there is no evidence of sliding or of filling material. For faults and dykes the flux of fluid due to an applied pressure gradient is determined primarily by the properties (porosity, permeability) of the material filling the crack and a (well understood) porous medium flow model is appropriate for describing the flow within the crack, see Bear [27]. Contrastingly, the pressure driven flow within joints is determined by the properties and orientation of the fractured surfaces, and is much less understood, in spite of the great deal of experimental and theoretical work done on such flows. An excellent summary of much of this work can be found in Cook [28] and features relevant to our context will be briefly described here.

Standard lubrication theory determines the flow between plates of separation distance (or aperture) W due to an applied pressure gradient p_x being proportional to the pressure gradient p_x, and the cube of the aperture W. Explicitly

$$Q = -\frac{p_x}{12\mu}W^3, \tag{1}$$

where Q is the fluid flow per unit length normal to the flow between the plates and μ is the dynamic viscosity, see Batchelor [29]. This result is referred to as Reynold's equation. The flow in geological joints is different in that asperities make contact between the crack walls so that the flow is tortuous and partially blocked. Nevertheless experiments performed by Witherspoon et al. [30] on artificially created joints in granite, basalt and marble show that for pressures up to 20 MPa, and apertures in the range 10 μm up to about 5 mm (the upper width range) the cubic law holds, see Fig. 6(a). These experiments also show that for apertures from 10 μm down to 6 μm (the middle range) the specific flow decreases less rapidly than W^3, and for (lower range) apertures less than 6 μm the specific minimum flux tends to a 'irreducible flow' limit independent of aperture. The explanation for the irreducible flow limit appears to be that under the higher normal pressures required for smaller separation there is little further increase in aspirates contact area and also in the size of larger voids so that the tortuosity and effective sectional area of flow does not change much with decreasing apertures. Other experiments by Engelder and Scholz [31] and Gale [32] however indicate a more rapid decrease in flux with width in the upper width range ($Q \propto W^n$ with n up to about 7.5), with a pronounced middle range ($n \approx 1.5$) and with a lower range irreducible flow limit similar to Witherspoon et al., see Fig. 6(b) and (c); note that the results do however vary significantly even with the same rock type. One way to deal with this variability in behaviour is to use a modified power law

$$Q = -a_n\frac{p_x}{12\mu}W^n \quad \text{with } 1 < n < \approx 7.5, \tag{2}$$

where both the power n and the coefficient a_n are dependent on rock type and geological history, and need to be determined experimentally. The 'linear' $n = 1$ case corresponds to the irreducible flow case. This approach has been used by Fitt et al. [33], and many others [28], and will be used here. There are alternative (more complex) models whose aim is to mechanistically understand joint flow behaviour especially in the middle and the lower aperture range, but a simple power law model will serve our purposes here.

In addition to the above complications there are crack network issues. The joints in rock form a huge and highly connected network through which the flow occurs, and furthermore there is a very strong dependence of flow on crack width. Under such 'network dominated' circumstances simple diffusion models fail, and various mathematical frameworks under the banner 'anomalous diffusion processes' have been used to attempt to describe the flow, see Ben-Avzaham and Halven [34]. Such models aim at

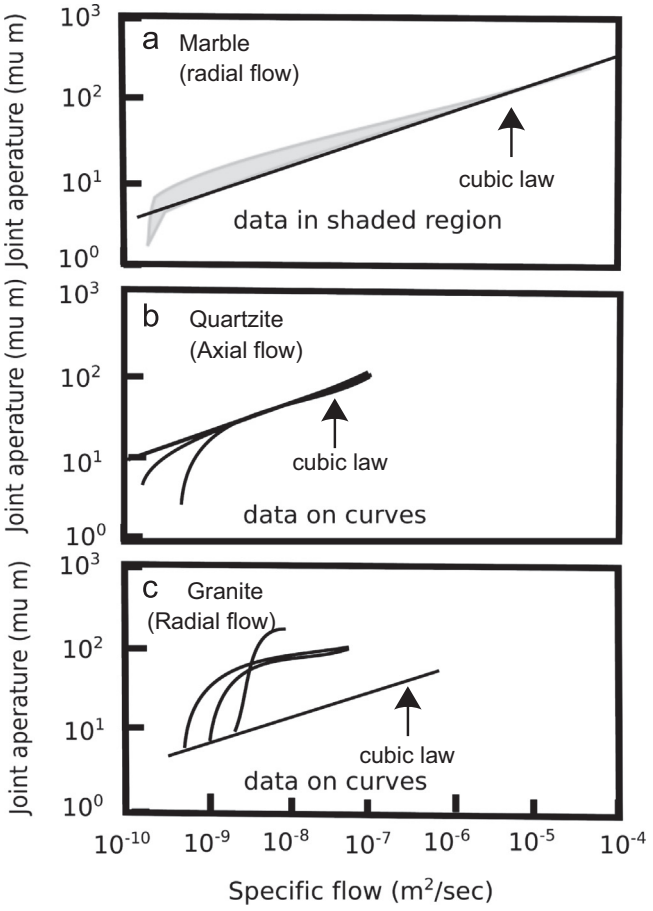

Fig. 6. (a) Experimental results by Witherspoon et al. showing the relations between specific flow $Q/\Delta h$ (flow per unit head) and joint aperture W. Results varied (slightly) with circumstances. In the upper range ($W > 10$ μm) we have $Q \propto W^3$. In the middle range (6–10 μm) $Q \propto W^n$ with $1 < n < 3$. In the lower range ($W < 6$ μm) the flux is independent of aperture, see Cook [28]. (b, c) Other results from Engelder and Scholz [36] and Gale [32]; results varied with the test run, see text.

reproducing/fitting the results without detailing the network. More recently attempts have been made to effectively describe the underlying network using self-similarity ideas, see Barabási [35], and are appropriate in strongly network dominated situations. These procedures so far have been used in social networks but may be useful in the present context. All such procedures require on-site experimental tuning. There have also been attempts to numerically model flows in a network of cracks, see for example Englman et al. [36], but the geometry of the connections is normally unknown and in the end one must rely on empirical fits. In the present context a detailed hydraulic model is not required so such on-site network issues will not be addressed; simple generic models will be examined. It is the time span for seepage from an abandoned mining shaft to a neighbourhood fault that is of central interest in this work. The simplest possible (2D) geometry is as shown in Fig. 7; we have flow up a planar crack at an angle θ to the horizontal intersecting a vertical shaft containing water. The crack may be identified as being a (thick) fault or dyke, or a (thin) joint. The water level in the shaft is measured from the intersection with the fault and to further simplify the analysis we consider the case in which the shaft continues to fill from above in such a way that height of the water remains fixed at H_w, and that initially the height of water in the crack is dry so that $h(0) = 0$, where $h(t)$ is the water height in the fault at time t measured from the junction. Evidently the water level in the fault will eventually reach H_w and our aim is to determine the dependence of this

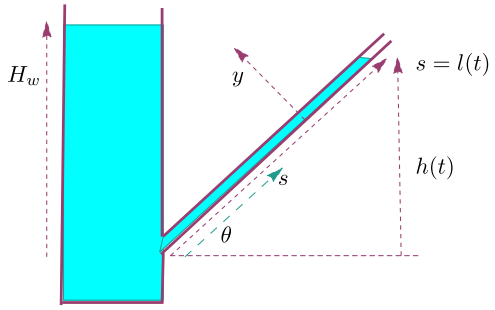

Fig. 7. Water flow up a crack of width W from a shaft. The crack may be thin (a joint) or thick (fault or dyke).

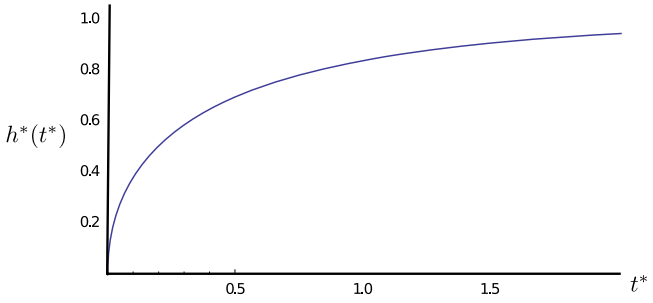

Fig. 8. The (scaled) hydraulically driven water movement $h^*(t^*)$ from a shaft into a fault.

characteristic time on the driving hydraulic head $\rho_w g H_w$ and the thickness W, length and orientation of the crack.

2.2. Flow up faults and dykes

As indicated above it is appropriate to model water flow in these cases as a porous medium flow between impermeable rock faces. The flow of a liquid through a porous medium can be studied by defining the piezometric head

$$\Phi = \frac{p}{\rho_w g} + z, \tag{3}$$

where z is the elevation above a datum here taken as the intersection of the fault with the shaft as in Fig. 7; p is the pressure, ρ_w is the water density and g is the gravitational acceleration. The usual model assumes that the flow is dictated by Darcy's Law [38,27], which states that the D'Arcy velocity (average volume flux) $\mathbf{u}$ is given by

$$\mathbf{u} = -\kappa \nabla \Phi, \tag{4}$$

where the hydraulic conductivity $\kappa = \rho_w g k/\mu$; here k is the coefficient of permeability of the material and μ is the dynamic viscosity of the fluid. The pressure at the bottom of the shaft is $\rho_w g H_w$, so the total potential of a particle at the bottom of the shaft is given by $\Phi(0) = H_w$. If $z = h(t)$ is the height of the column of water in the fault above the shaft base as shown in Fig. 7, then the total potential of a particle on the surface of this column is $\Phi(h) = h(t)$, so the driving potential in the fault is $(H_w - h(t))$ and the vertical flux $w = \kappa(H_w - h(t))/h(t)$, as given by (4). Now $w = h'(t)$, so that

$$\frac{dh}{dt} = \frac{\kappa(H_w - h)}{h} \quad \text{with } h(0) = 0 \tag{5}$$

if we assume the crack is initially dry. The appropriate scales to introduce are

$$h^\star = h/H_w, t^\star = t/T_f \quad \text{with } T_f = H_w/\kappa, \tag{6}$$

and with this choice (5) reduces to

$$\frac{dh^\star}{dt^\star} = \frac{1 - h^\star}{h^\star}, \tag{7}$$

with the implicit solution given by

$$t^\star = -\left[h^\star + \ln(1 - h^\star)\right], \tag{8}$$

plotted in Fig. 8.

During the initial filling stages the fault fills rapidly with

$$h^* \simeq (2t^*)^{1/2}, \quad \frac{dh^*}{dt^*} \simeq \frac{1}{(2t^*)^{1/2}} \quad \text{as } t^* \to 0, \tag{9}$$

and the level then slowly approaches the equilibrium level $(h^* = 1 - \exp(-t^*))$ as $t^* \to \infty$.

An estimate of the time for the crack to fill to 90% of the water depth in the shaft is obtained by letting $h^\star = 0.9$, giving an unscaled 'characteristic filling time' of

$$t_f = -T_f\left[0.9 + \ln(0.1)\right] \approx 1.5 T_f \quad \text{with } T_f = H_w/\kappa. \tag{10}$$

Notice that the characteristic time is independent of the crack angle and thickness; it is the flow between the particles filling the crack that dominates the flow.

The coefficient of permeability takes typical values of $\kappa \approx 1$ cm/s for gravel and $\kappa \approx 10^{-3}$ cm/s for fine sand, see Harr [38]. Assuming that the crack is filled with crushed matter approximating fine sand this gives an estimate time of $t_{90} \approx 1.5 T_f = 1.5 H_w/\kappa \approx 1.5 10^4/10^{-3} \approx 10^7$ s for $H_w \approx 300$ m, that is around 520 days. For 2000 m the estimated time is about 9.5 years. The fastest fill time would be of the order of days to weeks if the crack contained material with gravel-like properties, but this seems unlikely given the pressures at the depths of interest.

2.3. Flow up joints

It is appropriate to model this situation as channel flows between two walls separated by a distance of W, see again Fig. 7. As indicated earlier asperities connect the opposite wall faces and the flow is tortuous as a result, so that Reynolds cubic law connecting flux to aperture does not necessarily apply, however it is useful to first obtain results for the simpler planar walls channel flow case.

It is shown in the Appendix that the relevant equations integrate to give the fluid velocity along the fault, $u(y,t)$, as

$$u(y,t) = \frac{\rho_w g \sin\theta}{2\mu}\left[\frac{H_w}{h(t)} - 1\right] y(W - y), \tag{11}$$

with the associated flux of fluid along the fault given by

$$Q(t) = \int_0^W u(y,t)\, dy = \frac{\rho_w g \sin\theta}{12\mu}\left[\frac{H_w}{h(t)} - 1\right] W^3. \tag{12}$$

Note that the flux is proportional to W^3, and therefore satisfies the Reynolds cubic flow law, however this exact result quantifies the effect of joint orientation θ on the flow.

As indicated earlier in the tortuous flow case the joint can be replaced by a crack with regular parallel surfaces but with flux levels now proportional to $a_n W^n$, where $1 < n < \approx 7.5$, where n and a_n are empirical constants.

For the tortuous fault the fluid flux (12) becomes

$$Q(t) = \frac{\rho_w g \sin\theta}{12\mu}\left[\frac{H_w}{h_(t)} - 1\right] a_n W^n, \tag{13}$$

with the width averaged fluid velocity, $\overline{u}(t)$, defined by

$$\overline{u}(t) = \frac{1}{W}\int_0^W u(y,t)\, dy = \frac{\rho_w g \sin\theta}{12\mu}\left[\frac{H_w}{h(t)} - 1\right] a_n W^{n-1}. \tag{14}$$

using (13). Now $\overline{u}(t)$ is independent of the distance, s, along the fault and is therefore equal to the front speed of the fluid advancing up the joint. If $\ell(t)$ is the distance of the front from the joint point of the fault to the shaft, as illustrated in Fig. 7, then

$$\frac{d\ell}{dt} = \overline{u}(t). \tag{15}$$

But from Fig. 7, $\ell(t) = h(t)/\sin\theta$, so (15) may be expressed in terms of $h(t)$ as

$$\frac{dh}{dt} = \frac{\rho_w g \sin^2\theta}{12\mu}\left[\frac{H_w}{h(t)} - 1\right] a_n W^{n-1}; \tag{16}$$

an ordinary differential equation for the moving front. As with the fault flow case we introduce the dimensionless variables

$$h^* = \frac{h}{H_w}, \quad t^* = \frac{t}{T_j}, \tag{17}$$

with the characteristic time T_j now given by

$$T_j = \frac{12\mu H_w}{\rho_w g a_n W^{n-1} \sin^2\theta}. \tag{18}$$

With this choice (16) reduces to Eq. (7) obtained earlier for the filled fault case so that the solution (8) again applies with the unscaled filling time now given by

$$t_f = 1.5 T_j. \tag{19}$$

The crack filling process is thus similar for joints as for filled faults but with different time scales, given by (18) and (6). The significant difference is the fault angle θ dependence in the joint case.

2.3.1. Upper joint width range

In the Reynolds number cubic case we have $n=3$ and $a_3 = 1$, so that filling time increases very rapidly with decreasing fault thickness (like $1/W^2$) and varies in proportion to $1/\sin^2\theta$. With $\mu = 8.9 \times 10^{-4}$ Pa s, $\rho_w = 10^3$ kg/m^3, $g = 9.8$m/s^2 and $W=0.1$ mm we obtain 17–50 days as the fault angle decreases from 60° to 30°. For wider faults with $W=1$ mm we obtain hours rather than days, but such cracks are likely to be filled with crushed material. We noted earlier that some experimental results suggest values for n of up to about 7.5 for wide joints, so that the $n=3$ case provides an overestimate for the filling time for joints with aperture greater than about 10 μm, see (18). Wide cracks $W > 5$ mm (say) are in practice likely to be filled with granular material so that porous flow model is more appropriate in any case.

2.3.2. Intermediate and lower width range

In the intermediate aperture range (6–10 μm) we have $1 < n < 3$ with the smaller values of n corresponding to more tortuous flow. In this range $t_f \propto 1/W^{n-1}$ and therefore the filling time t_f increases with decreasing fault thickness although at a slower rate than for the Reynolds flow case. In lower width range (< 6 μm) we have $n = 1$ and the flow and filling times remains fixed with decreasing W.

To obtain estimates for the characteristic time in these cases we note that

$$\frac{t_f^{(n)}}{t_f^{(3)}} = \frac{W^{3-n}}{a_n}, \tag{20}$$

see (18) where a_n is independent of W, and needs to be determined experimentally.

2.4. Summary and observations

A summary of the results obtained for the both faults and dykes, and joints is presented in Table 1, using the Witherspoon experimental results (Fig. 6(a)), together with Eqs. (10), (18), and (20). The characteristic time in each case increases in direct proportion to the shaft depth H_w; in all results presented here $H_w = 2000$ m has been used, and 5 mm has been defined as the fault/joint dividing line.

As can be seen the characteristic time ranges from minutes to decades depending very strongly on the width of the crack and whether or not the crack is filled with particles. Note especially that the characteristic time for a 5 mm crack will be of the order of minutes if the crack is unfilled but can be up to about 10 years if the crack is filled with fine sand-like material.

Of course the fault is unlikely to directly connect up with the shaft as depicted with our simple generic model. There will likely be a network of joints of various sizes connecting the two, and there will also normally be a network of connecting shafts at the mining site. A complete hydrological model under such circumstances would require a useful (mathematical) description of the crack network and at present no such description is available, and of course on-site measurements (e.g. water depths in nearby shafts) would be necessary to tune the model parameters. However the above characteristic times for our generic model may be used to infer features of the hydraulic connection for specific cases. For example an effective crack width may be inferred based on the initial hydraulic response. It is evident from the above results that the thicker connecting cracks will determine the initial hydraulic response time and that the effective hydraulic conductivity will vary as more cracks in the network become filled. Such results may be used to assess the hazard posed by water accumulation and seepage from mining sites. We will illustrate using the observations sited in the Introduction.

As noted in the introduction there was a 14 month delay before seismic activity was recorded in the Goldbach abandoned mine example. Evidently because of the previous mining activities there were many potential slip planes in the old mine and many seismic vibrations from the production mine to trigger Type B events in the old mine, so that this time delay is associated with drainage. Such a time delay would be expected if the effective thickness of joints connecting through to the slip site were of the order of 12 μm, see Table 1 and Eq. (18) (mine depth approximately 2000 m).

In the Rocky Mountain Arsenal case a seepage response time of the order of 1 month was recorded which means that the joint network contains joints of effective thickness about 40 μm, see Table 1. In the Matsushiro experiment case the response time was of the order of 9 days corresponding to a thickness of about 0.1 mm (100 μm).

It should be noted that, due to the irreducibility of the flow as recorded in experiments, even for the very smallest joints (thickness 4 μm) the characteristic response times are of the order of decades for distances of the order of 2–3 km. Thus from a practical

Table 1
Characteristic times for a shaft depth of $H_w = 2000$ m for different width cracks. The inequality signs indicate that the estimate is likely to underestimate ($\leq$) or overestimate ($\leq$).

Crack width and type	t_f with $\theta = 60^\circ$	t_f with $\theta = 30^\circ$
> 5 μm fault (fine sand)	9.5 years	9.5 years
5 mm joint ($n=3$)	3 min	9 min
1 mm joint ($n=3$)	1.2 h	3.6 h
0.1 mm joint ($n=3$)	5 days	15 days
40 μm joint ($n=3$)	1 month	3 months
20 μm joint ($n=3$)	4.2 months	1 year
10 μm joint ($n=3$)	1.4 years	4 years
8 μm joint ($n=1.5$)	2 years	6.5 years
6 μm joint ($n=1.5$)	4 years	11.5 years
< 4 μm joint ($n=1$)	8.6 years	26 years

point of view one must assume that water will 'fill' all connecting cracks within a 2 km distance from the mining site.

The above calculations are based on Witherspoon's experiments using marble, but the results are typical especially in the medium to small aperture range. The irreducible flow level will however be dependent on the rock type and circumstances of joint formation so that experiments should be performed on-site to determine this important limit in specific cases.

3. Fault slip

In order to determine the effect of water seepage on fault slip we need to first identify the orientation of planes along which slip can occur under dry conditions, which will depend on the nature of the support for the geological structure, and this needs to be modelled. A suitable generic pre-mining stress model is presented in Section 3.1. Based on this model the conditions for fault slip are then determined first under dry conditions in Section 3.2. To determine the effect of water on fault slip a friction model is required; the classical Amonton friction model is used, see Section 3.3. The effect of the water is to increase the loading on the fault surfaces so that critical conditions for slip are modified, see Section 3.4. The slip planes are modelled to be planar (but with asperities) with prescribed (dry) frictional coefficient μ_0 in our generic model.

3.1. A pre-mining stress model

In regions excluding tunnels and faults the equations of static equilibrium and the compatibility equation for the Earth's stresses are given by

$$\tau_{xx,x}+\tau_{xy,y}=0, \tag{21}$$

$$\tau_{yy,y}+\tau_{xy,x}=-\rho_r g, \tag{22}$$

$$\nabla^2(\tau_{xx}+\tau_{yy})=0, \tag{23}$$

where the x-axis is horizontal, the y-axis vertically upwards measured from the Earth's surface and ρ_r is the rock density. Here τ_{ij} is the Cauchy stress tensor acting on the ith face in the jth direction. Assuming an initial relaxed stress state (that is with no unresolved shear) we have

$$\tau_{xx,x}=0, \quad \tau_{yy}=-\rho_r g y, \quad \tau_{xy}=0.$$

The driving force in the vertical direction is of course gravity, so the vertical normal stress is hydrostatic. Note however the horizontal variation in stress τ_{xx} is undetermined under equilibrium conditions until one specifies boundary conditions at $x\to\pm\infty$; one must specify how the geological structure is horizontally supported. Of course the support mechanism is very dependent on the formation and subsequent history of the geological structure, and sedimentary rock formations and volcanic rock formations are likely to be supported in very different ways. There is also considerable uncertainty as far as any formation is concerned, and very little available structural data to work with. Furthermore there are normally cracks throughout the structure so that the effective elastic properties are not those of a simple solid and will change with time; any geological structure will in fact continuously creep. Heim has suggested that under such conditions the stress distribution will tend towards hydrostatic, a situation referred to as *lithostatic*. Under such circumstances $\tau_{xx}=\tau_{yy}=-\rho_r g y$; a result that is referred to as Heim's Rule. If, on the other hand, the structure is unconstrained horizontally so that it is entirely self-supporting then $\tau_{xx}=0$. The region of interest may be either compressed or stretched by its containing vessel, however fractured rock is weak under tension so that under geological conditions only compression seems sustainable; under tension the material would crack thus releasing the tension. In order to model a range of practical geological circumstances we will use a 'k' model given by

$$\tau_{xx}=-k\rho_r g y, \quad \text{with } 0\le k\lesssim 2; \tag{24}$$

one would expect stresses to scale up 'hydrostatically'. One would expect $k\approx 1$ for sedimentary formations with k either smaller or larger under various external lateral loading. For self-supporting structures $k\approx 0$. Normally rocks are weak under tension so negative values of k are unlikely to occur. A database of in situ stresses in the Earth's crust in South Africa prior to any man-made disturbances is found in the Southern African Stress Database [39] part of which is shown in Fig. 9. It can be seen from this figure that there is a large variability without any visible trends, except a relationship with increasing depth, with all stress components increasing linearly with depth. Our simple 'k' model effectively describes such situations with the approximate practical range for k being $0.5<k\lesssim 2$. This generic model may be used to describe the local on-site stress variations with 'k' fitted appropriately using the Database or local knowledge. (For example if the angular displacement of a recent plane of slip and the coefficient of friction is known, then k can be inferred using results developed later, see (26).) A description of the database together with a range of other models appropriate for mining purposes can be found in Handley [40].

Mining will of course affect the stress distribution locally and more importantly will affect the loading on faults. In regions close to excavations the fault will be unloaded, and so more likely to slip. Such considerations are important in the present context and such issues have been addressed elsewhere, see Fowkes et al. [41]. Here we will avoid such complications.

3.2. Fault slip under k loading in the absence of water

If (X,Y) are the stresses acting on the vertical and horizontal faces of a wedge of rock ABC in contact with a fault/slip plane at angle θ to the horizontal, and (N,S) are the normal and shear stresses acting on the wedge across the fault face as in Fig. 10, then (with the adopted sign convention) horizontal and vertical static equilibrium conditions for the wedge require

$$N\sin\theta+S\cos\theta=X\sin\theta,$$

$$N\cos\theta-S\sin\theta=Y\cos\theta,$$

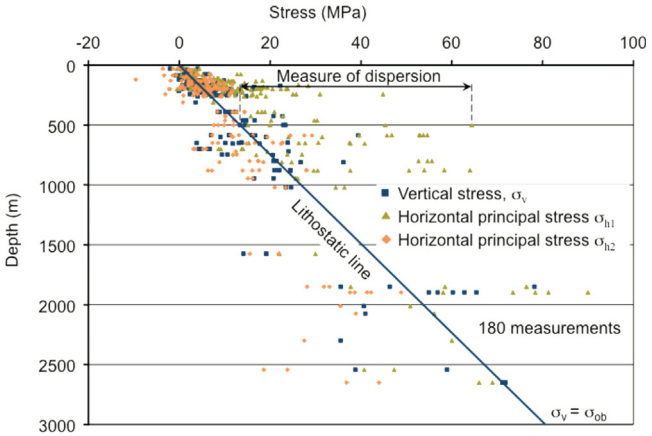

Fig. 9. Plot of measured stress data as a function of depth as recorded in the Southern African Stress Database.

in the limit as the wedge size goes to zero. Solving for (N,S) we obtain

$$N = X\sin^2\theta + Y\cos^2\theta, S = (X-Y)\sin\theta\cos\theta$$

Now $X \equiv -\tau_{xx}$ and $Y \equiv -\tau_{yy}$, with $X = k\rho_r gH$, $Y = \rho_r gH$ for our 'k' model, so the normal and shear forces acting across the fault face are given by

$$N/(\rho_r gH) = k\sin^2\theta + \cos^2\theta,\ S/(\rho_r gH) = (k-1)\sin\theta\cos\theta, \tag{25}$$

plotted in Fig. 11 for $0 < k < 2$ over the wedge angle range $0 \le \theta \le \pi/2$. The wedge will slip if $|S| > \mu_0 N$ where μ_0 is the frictional coefficient, that is if $\mu_0 < \mu_{\text{crit}}$ where the 'slip function'

$$\mu_{\text{crit}}(k,\theta) = \frac{|(1-k)|\ \sin\theta\cos\theta}{\cos^2\theta + k\sin^2\theta}, \tag{26}$$

defines our critical slip condition. Various scenarios are possible depending on the fault loading as defined by the value of k. Note that, see Fig. 11,

- $S > 0$ if $k > 1$, and (under such vessel compression circumstances) the wedge will slip up the fault plane for sufficiently small μ_0.
- $S < 0$ if $k < 1$, and the wedge will slip (gravitationally slide) down the fault plane for sufficiently small μ_0.
- Under lithostatic conditions $k = 1$ so $S = 0$ and the wedge will not slip irrespective of wedge angle and μ_0. Under such circumstances the force transmitted across the fault is always normal to the fault face.
- The normal stress N acting on the wedge increases as the wedge angle θ increases in the $k > 1$ (that is higher than lithostatic compression) case, and decreases in the case in which the region is under less than lithostatic compression. In the lithostatic $(k = 1)$ case N remains fixed as the wedge angle varies.

By plotting the slip function $\mu_{\text{crit}}(\theta)$ one can identify the fault angle range $(\theta_{\min}(\mu_0) < \theta < \theta_{\max}(\mu_0))$ corresponding to a prescribed μ_0.

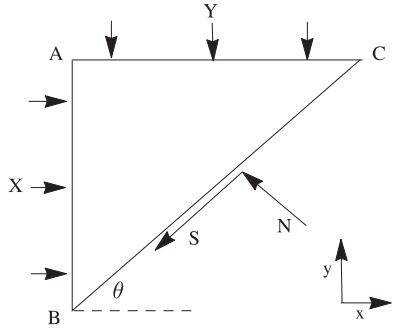

Fig. 10. Stresses acting on a wedge of rock ABC in contact with a fault plane BC at angle θ (in radians) to the horizontal.

In Fig. 12 the slip function is plotted out as a function of wedge angle for a small k case and a large k case. For decreasing μ_0 in the $k \gg 1$ (large compression) case slip first occurs (up the plane) for small fault angles, whereas in the $k \ll 1$ (gravity driven) case slip first occurs (down the plane) for large fault angles. In almost lithostatic $(k \approx 1)$ cases faults at an angle of $\pi/4$ first slip.

3.3. Friction models: the dry rock case

Rough surfaces (including rock faces) make contact only at high points called asperities, so that the real contact area between the surfaces is very much less than the apparent area (ratios of the order of 10^{-3} are typical under atmospheric pressure conditions), and the associated real stresses (real force/real contact area) are correspondingly very large, see Persson [42]. The asperities in contact compress or crush each other to the extent required to support the load and it is classically assumed (Amonton's rule) that the real normal stress remains fixed with increased loading and is given by the yield stress σ_{crit}. (Experimentally one finds that there is a slow increase in real normal stress with increasing loading until a plateau is reached, see [42].) Thus the Amonton model assumes that the normal stress N acting on the fault plane and the fractional contact area between the two faces A_{real} are related by

$$N = A_{\text{real}}\sigma_{\text{crit}}; \tag{27}$$

where σ_{crit} can be determined experimentally and so A_{real} can be inferred for prescribed loading. At a depth D below the Earth's surface the 'hydrostatic' rock pressure due to rock of density ρ_r is $\rho_r gD$ so that under such conditions the (fractional) real area of contact across a surface would be

$$A_{real} = \rho_r gD/\sigma_{crit}. \tag{28}$$

Typical values for σ_{crit} are 200–500 MPa for limestones and marbles [47], and with $\rho_r = 3.10^3$ kg/m^3 (granite) this gives a (fractional) real area of contact $A_{real} \approx 0.17$ at $D = 3000$ m.

Slip involves shearing of the asperities or gouging, so that slip conditions can be related back to the shear strength τ_{crit} of the material; we have

$$|S_{\max}| = A_{\text{real}}\tau_{\text{crit}}, \tag{29}$$

and since both N and $S_{\max}$ act over A_{real} *under dry contact*, we have

$$\tau_{\text{crit}} = \mu\sigma_{\text{crit}},$$

where μ is the observed coefficient of friction. The above 'rules' of frictional behaviour are referred to as Amonton's first and second laws. These rules/laws were first established and verified in metal contact (engineering) contexts where contact areas are relatively small and elastic or elasto-plastic forces dominate, but were found to work in much higher contact circumstances where adhesive forces play a role, see Persson [42]. They are also known to work in brittle rock situations, and so are generally assumed to work in fault slip contexts although geological pressure levels are much

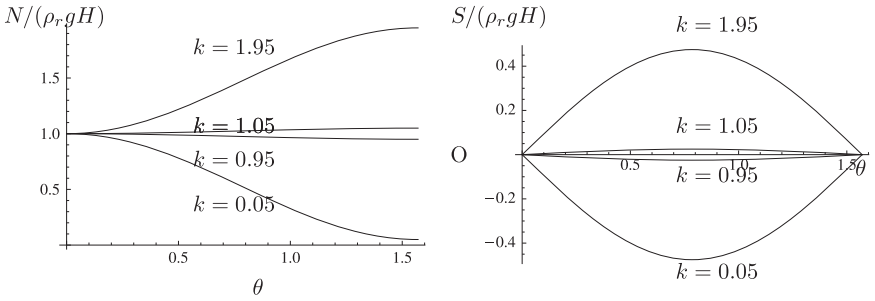

Fig. 11. The normal and shear forces acting on a fault at angle $0 < \theta < \pi/2$, for $k = 0.05, 0.95, 1.05, 1.95$: Left: $N(k,\theta)/(\rho_r gH)$. Right: $S(k,\theta)/(\rho_r gH)$.

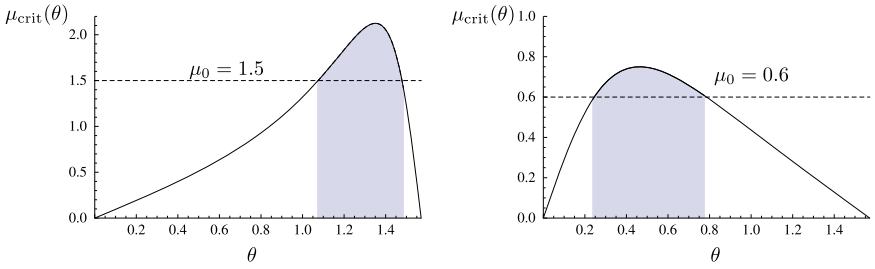

Fig. 12. The slip function: Left: a small k case ($k=0.05$). The slip fault angle range corresponding to $\mu_0 = 1.5$ is shaded. Right: a large k case ($k=4$). The slip fault angle range corresponding to $\mu_0 = 0.6$ is shaded.

larger and the contact surfaces are polished by previous movements, see Scholz [43,46] and Paterson and Wong [47].

Theoretical results have been obtained determining the real contact area as a function of real normal stress in terms of the roughness power spectrum and elastic/adhesive properties of the material, see Persson [42], but there appears to be no experimental verification for these results in the geological context. For more details see Greenwood and Williamson [44], Greenwood and Tripp [45], and for a recent review of contact theories see Persson [42]. We will use the Amonton model here.

One might ask if rocks behave like 'normal rocks' at the pressures of interest. The mine depths in South Africa are of the order of 2000–3000 m so hydrostatic (rock) pressure levels of the order of 40–90 MPa (using $\rho_r = 2\text{–}3 \times 10^3$ kg/m^3, $g = 9.8$ m/s^2) are expected, see Scholz [46]. The yield stress of rocks (silicates) is of the order of 500 MPa, so one would not expect 'global plastic' behaviour of rocks at 3000 m. The yield stresses are affected by temperature and pressure, both of which are large at the depths of interest, however in context the effects are marginal, see Scholz [46].

3.4. Slip after water entry

Water entering a fault will fill the 'free' (non-real rock contact) spaces. Under equilibrium water flow conditions this water will be at hydrostatic pressure $\rho_w g H_w$, where H_w is the depth of water at the location of interest. At depths of the order of 2000–3000 m this will be approximately 30 MPa, and roughly one-third the rock pressure. This water will take up part of the applied elastic stress N normal to the fault, thus reducing the fractional area of real contact between the opposing faces from $A_0 \equiv A_{real}$ (corresponding to dry conditions at depth D) to A_w (under hydrostatic loading). Since the same normal force N needs to be supported as before, we have, from (27),

$$N = A_w \sigma_{\rm crit} + (1 - A_w)\rho_w g H_w = A_0 \sigma_{\rm crit},$$

which determines the real area of contact under hydrostatic loading as

$$\frac{A_w}{A_0} = 1 - \left(\frac{1 - A_0}{A_0}\right)\left(\frac{\Psi}{1 - \Psi}\right), \tag{30}$$

where

$$\Psi = \frac{\rho_w g H_w}{\sigma_{\rm crit}} \text{ and } A_0 = \frac{\rho_r g D}{\sigma_{crit}}, \tag{31}$$

see (28).

Resistance to applied shear can only be provided by the contacting asperities (since water cannot provide resistance to shear under static loading), so that the maximum externally applied shearing force that can be resisted under hydrostatic loading will be reduced from $A_0 \tau_{\rm crit}$ to $A_w \tau_{\rm crit}$, and thus the effective coefficient of friction under hydrostatic loading will be reduced in proportion to the contact area ratio and we have

$$\frac{\mu_w}{\mu_0} = \frac{A_w}{A_0} = 1 - \left(\frac{1 - A_0}{A_0}\right)\left(\frac{\Psi}{1 - \Psi}\right), \tag{32}$$

using (30). The effect of water entry on the effective frictional coefficient is thus determined by the two scaled hydrostatic pressures (A_0, Ψ) (water and rock) at the location on the fault, where the appropriate scale to use is the yield stress of the rock $\sigma_{\rm crit}$. It should be noted that the correction factor in (32) consists of an area ratio term multiplied by a hydraulic term. We have used the Amonton model to determine A_0 and thus the area ratio term, see (31), but an improved contact area model for A_0 as a function of hydrostatic rock pressure could be used here.

Both scaled hydrostatic pressure parameters are relatively small (0.17, 0.06) for mining depths of interest (3000 m) so that (32) can be approximated by

$$\frac{\mu_w}{\mu_0} \approx 1 - \frac{\Psi}{A_0} = 1 - \frac{\rho_w}{\rho_r}\frac{H_w}{D}, \tag{33}$$

which reaches a maximum value of $(1 - \rho_w/\rho_r) \approx (1 - 0.30)$ if $D = H_w$; a 30% change in μ_w/μ_0. Note that the effective frictional coefficient decreases almost linearly with water depth H_w for mining depths of interest.

Now of course whether a particular fault slips as a result of water inflow will depend on just how close it was to sliding in the first place, and we have seen that this depends on the orientation θ of the fault and the local stress field as specified by k. For illustration in Fig. 13 we examine the water entry effect in the $k=0.05$ case displayed earlier in dry conditions, with water depths of 2000 m and 3000 m. Note especially that not only are fault planes within the dry failure θ range more prone to slip but most significantly also new θ planes of weakness become slip prone. Undoubtedly this would result in an increased incidence of Type B seismic events and it would be useful to theoretically quantify this

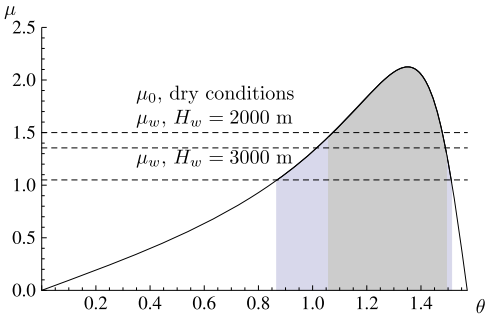

Fig. 13. Water entry effects in the $k=0.05$ case with $\mu = 1.5$ under dry conditions (upper dashed line) and corresponding μ_w values for water depths of $H_w = 1000$ m (middle dashed line) and $H_w = 3000$ m (lower line). Note especially that the range of fault angles (here measured in radians) for slip is increased significantly after water entry.

change. In order to do this one would need to know the distribution function $N(\theta)$ for fault planes at the specific site. This would be strongly dependent on the geological history of the site as well as its present state; on-site observations of seismic events would be required. A *very* crude estimate can be obtained by assuming a uniform distribution function in which case the increased incidence can be obtained by simply comparing the θ range for slip before and after water entry which can be obtained using the slip function (26). For the $k=0.05$ case displayed in Fig. 13 the θ intervals for slip can be read off and a 50% incidence increase is indicated. Whilst this may seem large it should be noted that in the Goldbach abandoned mine example observations indicate a very large incidence increase, see Fig. 4.

4. Results and discussion

The observations documented by Goldbach [20] provided compelling evidence that seepage from abandoned mines can significantly increase Type B seismic events in the mining region. The present work examined simple models of the processes involved and the quantitative results obtained are consistent with these observations.

The first issue was whether water would seep through to faults in the mining district in a time span of concern, say 10 years. Based on the considerable and reliable experimental database and robust models we found that the characteristic time span for seepage over a distance of order of 3000 m ranges from weeks for faults, up to about 10 years for very thin joints, see Table 1. The result for very thin joints was somewhat surprising and arises because of the observed 'irreducible' flow limit through such joints. Evidently on-site experimental observations would be necessary to determine the hydrology of a particular mining site, but the above results do provide useful estimates for the characteristic times involved, and these results indicate that it is *very likely* that water will leak into faults within 3000 m of the site over time spans of months as has been observed in flooded sites.

The second issue was whether slip would be more likely on the hydraulically loaded faults at depths of the order of present deep mines (3000 m). Slip will occur along a fault if the modulus of the shear force is sufficiently large compared with the normal force, a result that is quantified in (26). This result depends on the fault angle θ and the local fault loading quantified here by k, see (24), which may be estimated for a particular site using the South African Stress Database [40]. The effect of hydraulic loading on this result was determined using Amonton's rule model which leads to a result for the effective coefficient of friction for the water filled fault, see (33). The effective coefficient of friction was found to decrease in proportion to the water depth at the location, and 20–30% reductions are possible. Furthermore (and importantly) the range of fault angles prone to slip is greatly increased as a result of water entry, with angles both greater than and less than those previously active becoming prone to slip. The significantly increased incidence of seismic events after flooding seen in the Goldbach abandoned mine example might therefore be expected, see Fig. 4.

These results certainly suggest strongly that allowing the old deep mines to fill with water is very likely to significantly increase seismic incidence. The above theoretical models are generic and crude and observations of seismic activity in abandoned mines are limited; evidently more detailed observational work involving both hydrological and seismic on-site measurements is indicated. A JAGUARS type network in an abandoned mine would be ideal to separate out Type B events from 'normal' Type A events and to determine the increased incidence distribution function.

Acknowledgements

The authors would like to acknowledge that the reviewers' detailed suggestions, particularly in regard to observational data, have lead to a very much improved paper.

Appendix A. Reynolds flow along a long thin fault

In this Appendix, Reynolds flow along a long thin fault without surface roughness or touching asperities will be considered. The fluid pressure and the fluid velocity will be derived. The results will be adapted in Section 2.2 to the flow along a thin fault with surface roughness and contact areas.

The mine shaft and fault are illustrated in Fig. 1. Since the fault is long and thin we will make the lubrication approximation that inertia can be neglected. This approximation will be valid if conditions (6) in the manuscript are satisfied. The thin fluid film equations are [37]

$$\frac{\partial p}{\partial s}=\mu\frac{\partial^2 u}{\partial y^2}-\rho_w g\sin\theta \tag{A.1}$$

$$\frac{\partial p}{\partial y}=-\rho_w g\cos\theta \tag{A.2}$$

$$\frac{\partial u}{\partial s}+\frac{\partial v}{\partial y}=0 \tag{A.3}$$

where s is the distance along the fault measured from the junction point of the fault with the shaft, y measures the perpendicular distance from the lower fault surface, $p(s,y,t)$ is the fluid pressure in the fault and $u(s,y,t)$ and $v(s,y,t)$ are the components of the fluid velocity in the fault. In the thin fluid film approximation v is of order $u, W/H_w$. We will make the approximation that $v(s,y,t)=0$. It then follows directly from (A.3) that $u=u(y,t)$.

Consider first the fluid pressure $p(s,y,t)$. From (A.2),

$$p(s,y,t)=-\rho_w g\cos\theta+A(s,t) \tag{A.4}$$

and (A.1) becomes

$$\frac{\partial A}{\partial s}(s,t)=\mu\frac{\partial^2 u}{\partial y^2}(y,t)-\rho_w g\sin\theta. \tag{A.5}$$

Differentiating (A.5) with respect to s gives

$$\frac{\partial^2 A}{\partial s^2}(s,t)=0 \tag{A.6}$$

and therefore

$$A(s,t)=sB(t)+C(t). \tag{A.7}$$

Eq. (A.5) becomes

$$B(t)=\mu\frac{\partial^2 u}{\partial y^2}-\rho_w g\sin\theta \tag{A.8}$$

and from (A.4),

$$p(s,y,t)=sB(t)+C(t)-\rho_w g\cos\theta. \tag{A.9}$$

The boundary conditions are imposed on $\overline{p}(s,t)$, the fluid pressure averaged over the width of the fault. We have

$$\overline{p}(s,t)=\frac{1}{W}\int_0^W p(s,y,t)\mathrm{d}y=sB(t)+C(t)-\frac{1}{2}\rho_w gW\cos\theta. \tag{A.10}$$

The boundary conditions on $\overline{p}(s,t)$ are

$$s=0:\quad \overline{p}(0,t)=p_A+\rho_w gH_w, \tag{A.11}$$

$$s=\ell(t):\quad \overline{p}(\ell(t),t)=p_A, \tag{A.12}$$

where p_A is the atmospheric pressure and $\ell(t)$ is the length of the fluid in the fault. Thus

$$B(t) = -\frac{\rho_w g H_w}{\ell(t)}, \tag{A.13}$$

$$C(t) = p_A + \rho_w g H_w + \frac{1}{2}\rho_w g W \cos\theta, \tag{A.14}$$

and therefore

$$\overline{p}(s,t) = p_A + \rho_w g H_w \left[1 - \frac{s}{\ell(t)}\right]. \tag{A.15}$$

Consider next the fluid velocity $u(y,t)$. From (A.8) and (A.12),

$$\frac{\partial^2 u}{\partial y^2} = -\frac{\rho_w g \sin\theta}{\mu}\left[\frac{H_w}{\ell(t)\sin\theta} - 1\right], \tag{A.16}$$

and therefore

$$u(y,t) = -\frac{\rho_w g \sin\theta}{2\mu}\left[\frac{H_w}{\ell(t)\sin\theta} - 1\right] y^2 + yD(t) + E(t). \tag{A.17}$$

Imposing the no slip boundary conditions

$$u(0,t) = 0, \quad u(W,t) = 0, \tag{A.18}$$

we obtain

$$u(y,t) = \frac{\rho_w g \sin\theta}{2\mu}\left[\frac{H_w}{\ell(t)\sin\theta} - 1\right] y(W-y). \tag{A.19}$$

We express $u(y,t)$ in terms of $h(t)$, the height of the fluid front above the joint point of the fault to the mine shaft. From Fig. 1

$$\ell(t) = \frac{h(t)}{\sin\theta} \tag{A.20}$$

and therefore

$$u(y,t) = \frac{\rho_w g \sin\theta}{2\mu}\left[\frac{H_w}{h(t)} - 1\right] y(W-y). \tag{A.21}$$

Eq. (A.21) is the result for the fluid velocity which will be required in Section 2.2

References

[1] Gibowicz SJ, Lasocki S. Seismicity induced by mining: ten years later. Adv Geophys 2000;44:39–167.
[2] Durrheim RJ. Mitigating the risk of rockbursts in the deep hard rock mines of South Africa: 100 years of research. In: J. Brune, editor. Extracting the science: a century of mining research. Arizona: Society for Mining, Metallurgy, and Exploration, Inc.; 2010. p. 156–71.
[3] Jager AJ, Ryder JA. A handbook on rock engineering practice for tabular hard rock mines safety in Mines Research Advisory Committee, Johannesburg; 1999.
[4] Cook NGW, Hoek E, Pretorius JPG, Ortlepp WD, Salamon MDG. Rock mechanics applied to the study of rockbursts. J S Afr Inst Min Metall 1966;66:435–528.
[5] Gay NC, Spencer D, Van Wyk JJ, Van Der Heever PK. The control of geological and mining parameters in the Klerksdorp Gold Mining District. In: Gay NC, Wainwright EH, editors. Proceedings of the first international congress on rockbursts and seismicity in mines, Johannesburg, 1982. Johannesburg: SAIMM; 1984. p. 107–20.
[6] Lawrence D. Seismicity in the Orange Free State gold-mining district. In: Gay NC, Wainwright EH, editors. Proceedings of the first international congress on rockbursts and seismicity in mines, Johannesburg, 1982. Johannesburg: SAIMM; 1984. p. 121–30.
[7] Spottiswoode SM. Source mechanisms of mine tremors at Blyvooruitzcht gold mine. In: Gay NC, Wainwright EH, editors. Proceedings of the first international congress on rockbursts and seismicity in mines, Johannesburg, 1982. Johannesburg: SAIMM; 1984. p. 29–37.
[8] Potgieter GJ, Roering C. Source mechanism studies of mine-induced seismic events in a deep level gold mine. In: Gay NC, Wainwright EH, editors. Proceedings of the first international congress on rockbursts and seismicity in mines, Johannesburg, 1982. Johannesburg: SAIMM; 1984. p. 51–5.
[9] Ortlepp WD. Rockbursts in South African gold mines: a phenomenological view. In: Gay NC, Wainwright EH, editors. Proceedings of the first international congress on rockbursts and seismicity in mines, Johannesburg, 1982. Johannesburg: SAIMM; 1984. p. 165–78.
[10] Van Antwerpen HEF, Spengler MG. The effect of mining-related seismicity on excavations at East Rand Proprietary Mines, Limited. In: Gay NC, Wainwright EH, editors. Proceedings of the first international congress on rockbursts and seismicity in mines, Johannesburg, 1982. Johannesburg: SAIMM; 1984. p. 235–43.
[11] Deliac EP, Gay NC. The influence of stabilising pillars on seismicity and rockbursts at ERPM. In: Gay NC, Wainwright EH, editors. Proceedings of the first international congress on rockbursts and seismicity in mines, Johannesburg, 1982. Johannesburg: SAIMM; 1984. p. 257–63.
[12] Van Der Heever PK. Some technical and research aspects of the Klerksdorp seismic network. In: Gay NC, Wainwright EH, editors. Proceedings of the first international congress on rockbursts and seismicity in mines, Johannesburg, 1982. Johannesburg: SAIMM; 1984. p. 349–50.
[13] Richardson E, Jordan TH. Seismicity in deep gold mines of South Africa: implications for tectonic earthquakes. Bull Seismol Soc Am 2002;92 (5):1756–82.
[14] Hanks TC, Kanamori H. A moment magnitude scale. J Geophys Res 1979;84:2348–50.
[15] Dieterich JH. Modelling of rock friction: experimental results and constitutive equations. J Geophys Res 1979;84:2161–8.
[16] Aki K. Magnitude frequency relation for small earthquakes. J Geophys Res 1987;93:1349–55.
[17] Kwiatek G, Plenkers K, Nakatani M, Yabe Y, Dresen G. Frequency-magnitude characteristics down to magnitude-4.4 for induced seismicity recorded at Mponeng gold mine, South Africa. Bull Seismol Soc Am 2010;100(3):1165–73.
[18] Kwiatek G, Plenkers K, Dresen G. Source parameters of pico seismicity recorded at Mponeng deep gold mine South Africa: implications for tectonic earthquakes. Bull Seismol Soc Am 2011;101:2592–608.
[19] Plenkers K, Kwiatek G, Nakatani M, Dresen G. Observation of seismic events with frequencies f 25 kHz at Mponeng deep gold mine, South Africa. Seismol Res Lett 2010;81(3):467–79.
[20] Goldbach OD. Seismic risks posed by mine flooding. In: Proceedings of the hard rock safe safety conference. Johannesburg: SAIMM; 2009.
[21] Healy JH, Rubey WW, Griggs DT, Raleigh CB. The Denver earthquakes. Science 1968;161(3848):1301–10.
[22] Raleigh CB, Healy JH, Bredehoeft JD. An experiment in earthquake control at Rangely Colorado. Science 1976;191:1230–6.
[23] Gibbs JF, Healy CB, Raleigh JM, Coakley JM. Seismicity in the Rangely Colorado area: 1962–1970. Bull Seismol Soc Am 1973;63:1557.
[24] Raleigh CB, Healy JH, Bradehoeft B. An experiment in earthquake control at Rangely Colorado. Science 1976;191(4233):1230–7.
[25] Ohtake M. Seismic activity induced by water injection at Matsushiro, Japan. J Phys Earth 1974;22:163–76.
[26] Brandt M. A review of the reservoir induced seismicity at the Katse Dam, Kingdom of Lesotho, November 1995 to March 1999. In: Van Aswegen G, Durrheim RJ, Ortlepp WD, editors. Proceedings of the fifth international symposium on rockbursts and seismicity in mines (RaSIM5), Johannesburg; 2000. Johannesburg: SAIMM; 2000, p. 119–32.
[27] Bear J. Dynamics of fluids in porous media. New York: Elsevier; 1972.
[28] Cook NGW. Natural joints in rocks; mechanical, hydraulic and seismic behaviour under normal stress. Int J Rock Mech Min Sci Geomech Abstr 1992;29:127–223.
[29] Batchelor GK. An introduction to fluid mechanics. London: Cambridge University Press; 1967. p. 179–83.
[30] Witherspoon PA, Wang JSY, Iwa K, Gale JE. Validity of the cubic law for fluid flow in a deformable rock structure. Water Resour Res 1980:1016–24.
[31] Engelder T, Scholz CH. Fluid flow along very smooth joints at effective pressure up to 200 megapascals: mechanical behaviour of crustal rocks. Am Geophys Union Mono 1981;24:147–52.
[32] Gale JE. A numerical, field and laboratory study of flow in rocks with deformable fractures [Ph.D. thesis]. Berkeley: University of California; 1975.
[33] Fitt AD, Kelly AD, Please CP. Crack propagation models for rock fracture in a geothermal energy reservoir. SIAM J Appl Math 1995;55:1592–608.
[34] Halvin S, Ben-Avraham D. Diffusion in disordered media. Adv Phys 2002;51:187.
[35] Barbabási AL. The new science of networks. New York: Perseus Book Group; 2002.
[36] Englman R, Gur Y, Jaeger Z. Fluid flow through a crack network in rocks. J Appl Mech 2009;50(4a):707–11.
[37] Acheson DJ. Elementary fluid dynamics. Oxford: Clarendon Press; 1990. p. 238–251.
[38] Harr M. Groundwater and seepage. New York: McGraw Hill; 1962.
[39] Stacey TR, Wesseloo J. In situ stresses in mining areas in South Africa. J S Afr Inst Min Metall 2013;98:365–8.
[40] Handley MF. Pre-mining stress model for subsurface excavations in southern Africa. J S Afr Inst Min Metall 113:449–71.
[41] Fowkes ND, Mason DP, Napier JAL. Fault slip in a mining context. In: Proceedings of the mathematics in industry study group South Africa; 2004. p. 1–21.
[42] Persson BNJ. Contact mechanics for randomly rough surfaces. Surf Sci Rep 2006;61:201–27.
[43] Scholz CH. Earthquake and friction laws. Nature 1998;391:37–42.
[44] Greenwood JA, Williamson GW. Multiasperity contact models. Proc R Soc Lond A 1966;295–300.
[45] Greenwood JA, Tripp J. The elastic contact of rough spheres. J Appl Mech Trans ASME 1976:153–9.
[46] Scholz CH. The mechanics of earthquakes and faulting. 2nd ed.Cambridge University Press; 2002.
[47] Paterson MS, Wong T. Experimental rock deformation—the brittle field. Berlin: Springer-Verlag; 2005.